

# Magnetic excitations in multiferroic $\text{LuMnO}_3$ studied by inelastic neutron scattering

H. J. Lewtas, A. T. Boothroyd,\* M. Rotter, and D. Prabhakaran

*Oxford University Department of Physics, Clarendon Laboratory, Parks Road, Oxford, OX1 3PU, UK*

H. Müller

*Institute for Solid State Physics, University of Technology Vienna, Wiedner Hauptstr 8-10, A-1040 Wien, Austria*

M. D. Le

*Helmholtz-Zentrum Berlin für Materialien und Energie,  
Hahn-Meitner-Platz 1, D-14109, Berlin, Germany*

B. Roessli and J. Gavilano

*Laboratory for Neutron Scattering, Paul Scherrer Institute, CH-5232 Villigen PSI, Switzerland*

P. Bourges.

*Laboratoire Léon Brillouin, CEA-CNRS, CE Saclay, 91191 Gif sur Yvette, France*

(Dated: August 4, 2010)

We present data on the magnetic and magneto-elastic coupling in the hexagonal multiferroic manganite  $\text{LuMnO}_3$  from inelastic neutron scattering, magnetization and thermal expansion measurements. We measured the magnon dispersion along the main symmetry directions and used this data to determine the principal exchange parameters from a spin-wave model. An analysis of the magnetic anisotropy in terms of the crystal field acting on the Mn is presented. We compare the results for  $\text{LuMnO}_3$  with data on other hexagonal  $\text{RMnO}_3$  compounds.

PACS numbers: 75.30.Ds, 75.25.Dk, 75.50.Ee, 75.85.+t

## I. INTRODUCTION

Multiferroic materials have been intensively studied in recent years following the discovery of compounds that display giant cross-coupling effects between magnetic and ferroelectric order parameters<sup>1-3</sup>. Particular interest has been aroused by the possibility of new magnetoelectric coupling mechanisms<sup>4-6</sup> and the potential for exploitation in technological applications<sup>7-9</sup>. One of the most investigated families of multiferroics is the hexagonal manganites  $\text{RMnO}_3$ , which form with  $R = \text{Sc, Y, Ho, Er, Tm, Yb and Lu}$ . The magnetoelectric behavior found in this family is associated with frustrated antiferromagnetic interactions of Mn spins on a triangular lattice. The compounds formed with  $R = \text{Sc, Y and Lu}$  are attractive for fundamental studies because they are not complicated by additional magnetic contributions from the  $R$  ions and because they form a family in which changes in structure and magnetoelectric behavior can be correlated in a systematic way. Here we focus on  $\text{LuMnO}_3$ , and present neutron scattering measurements of the cooperative magnetic dynamics and measurements of the thermal expansion by dilatometry. The data provide quantitative information on the exchange interactions, magnetic anisotropy, and magnetostriction, all of which play a part in the magnetoelectric coupling. The results are compared with similar measurements on  $\text{YMnO}_3$ .

The crystal structure of the hexagonal manganites, which is described by the space group  $P6_3cm$ , is built from corner-sharing  $\text{MnO}_5$  bipyramids which form layers parallel to the  $ab$  plane separated by rare earth ions, as

shown in Fig. 1. The Mn ions form a near-ideal triangular lattice. The ferroelectric distortion, which occurs at a high temperature ( $T_c > 1000 \text{ K}$  for  $\text{LuMnO}_3$ , Ref. 10), is caused by a tilting of the  $\text{MnO}_5$  bipyramids and a buckling of the  $R$  plane, which together create a  $\sqrt{3} \times \sqrt{3}$  superlattice distortion (trimerization) of the Mn ions and a ferroelectric moment along the  $c$  axis<sup>10,11</sup>. The distortion shifts the Mn ions along the  $a$  axis away from the ideal  $x = 1/3$  position<sup>12</sup> — see Fig. 1.

The magnetic properties of  $\text{LuMnO}_3$  arise from the (almost) triangular layers of  $\text{Mn}^{3+}$  ( $3d^4$ ) ions with  $S = 2$ . Neighboring spins are coupled by antiferromagnetic exchange interactions which are frustrated by the triangular geometry, as evidenced by the large ratio of the Weiss to Néel temperatures  $|\Theta/T_N| \sim 10$  (Ref.13), the anomalous magnetic entropy below  $T_N$ <sup>13</sup>, and the reduction in the value of the ordered magnetic moment to about 75% of the full spin-only moment for  $S = 2$  (Ref. 10). The Mn spins in all the hexagonal  $\text{RMnO}_3$  compounds form a classical  $120^\circ$  structure within the triangular layers (Fig. 1)<sup>10,14-18</sup>. The spins are confined by anisotropy to lie in the  $ab$  plane, and the large inter-layer separation decouples the layers electronically and makes the magnetism quasi-two-dimensional. In the case of  $\text{LuMnO}_3$ , magnetic ordering occurs below  $T_N = 88 \text{ K}$ .

Evidence for magnetoelectric coupling in  $\text{RMnO}_3$  compounds is provided by anomalies at  $T_N$  in the dielectric constant<sup>13,19</sup>, lattice dynamics<sup>20-23</sup>, thermal conductivity<sup>24</sup> and structural parameters<sup>25-27</sup>. There are also interesting observations by optical second-harmonic generation which show a cross-correlation between fer-

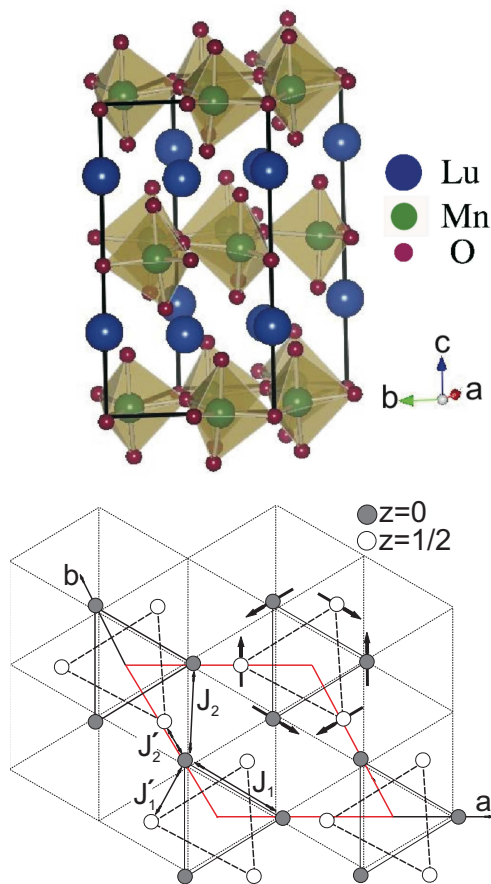


FIG. 1: (Color online) (a) The hexagonal layered structure of  $\text{LuMnO}_3$ . (b) Projection of the structure down the  $c$  axis showing the Mn sites. The large (red) diamond is the projection of chemical/magnetic unit cell, and the filled and empty circles represent Mn at fractional heights  $z = 0$  and  $z = 1/2$ , respectively. The Mn trimerization has been exaggerated for emphasis. The in-plane ( $J_1$ ,  $J_2$ ) and out-of-plane ( $J'_1$ ,  $J'_2$ ) Mn–Mn exchange couplings used in the spin-wave model are shown. Arrows on the Mn atoms show the probable magnetic structure of  $\text{LuMnO}_3$  based on neutron diffraction<sup>10</sup> and optical second harmonic generation<sup>17</sup>.

roelectric and magnetic domains due to the formation of magnetic domain walls below  $T_N$  which coincide with ferroelectric domain walls<sup>28–30</sup>.

The precise microscopic mechanism of the magnetoelectric coupling in  $\text{RMnO}_3$  has not been described yet. Careful structural measurements on  $\text{Y}_{1-x}\text{Lu}_x\text{MnO}_3$  have shown that an isostructural transition takes place at  $T_N$  (Ref. 26), which causes further displacements of the ions resulting in a small increase in the ferroelectric polarization. It was therefore proposed that the magnetoelectric coupling is driven by a primary magnetoelastic coupling. The origin of the magnetoelastic coupling, however, remains unclear. One possibility is that the isostructural distortion may occur in order to relieve some energy associated with magnetic frustration<sup>31</sup>. Another proposal

is that the system might benefit energetically from the Dzyaloshinskii–Moryia interaction below  $T_N$  via a small  $c$ -axis displacement in the oxygen atoms that bond adjacent Mn atoms<sup>32</sup>. This displacement would produce a small additional electric polarization along the  $c$  axis.

## II. EXPERIMENTAL

Single crystals of  $\text{LuMnO}_3$  were prepared by the optical floating-zone technique as follows. Polycrystalline  $\text{LuMnO}_3$  was prepared by standard solid-state reaction from high purity ( $>99.999\%$ )  $\text{Lu}_2\text{O}_3$  and  $\text{MnO}_2$ . The polycrystalline powder was pressed into rods of diameter 8 mm and length 80 mm, and sintered at  $1300^\circ\text{C}$  for 24 hours. Single crystals were grown in a four-mirror optical floating-zone furnace (Crystal Systems Inc.) at a scanning rate of  $3\text{--}4\text{ mm hr}^{-1}$  with the feed and seed rods counter-rotating at 30 rpm. The growth was performed in a flowing atmosphere of argon and oxygen in the ratio 12:1. At each stage in the preparation the phase purity of the product was checked by powder X-ray diffraction.

Unpolarized neutron scattering measurements were performed on a crystal of mass 1.9 g on the cold-neutron triple-axis spectrometer TASP at the SINQ facility (PSI, Switzerland) and on the thermal triple-axis 2T1 at LLB-Orphée (Saclay, France). At TASP, the crystal was mounted in an ‘orange’ helium cryostat and neutron spectra were recorded with a fixed final energy of 4.5 meV. The corresponding setup at 2T1 was with a closed-cycle refrigerator and a fixed final energy of 14.7 meV. Measurements were made with either  $a^*$  and  $c^*$  or  $a^*$  and  $b^*$  in the horizontal scattering plane, where  $a^*$ ,  $b^*$  and  $c^*$  are the axes of the hexagonal reciprocal lattice. On 2T1 some measurements were also made in the plane parallel to the  $a^*b^*$  plane but displaced by 0.5 reciprocal lattice units along the  $c^*$  axis. The lattice parameters of  $\text{LuMnO}_3$  referred to the space group  $P6_3cm$  are  $a = b = 6.05\text{ \AA}$ ,  $c = 11.4\text{ \AA}$ , and the inter-axis angles are  $\alpha = \beta = 90^\circ$ ,  $\gamma = 120^\circ$ . Hence,  $a^* = b^* = 4\pi/(a\sqrt{3})$ , and  $c^* = 2\pi/c$ .

Magnetic measurements were performed with a superconducting quantum interference device (SQUID) magnetometer on a small piece of crystal cut from the same rod as the neutron crystal. The thermal expansion was measured on the same piece of crystal with a miniature capacitance dilatometer<sup>33,34</sup>.

## III. RESULTS

Figure 2 shows the magnetization of  $\text{LuMnO}_3$  for a magnetic field of strength 1000 Oe applied parallel to the  $ab$  plane and along the  $c$  axis. Magnetic ordering is signalled by a sharp peak in the magnetization at  $T_N = 87.5 \pm 0.5\text{ K}$  (Fig. 2 lower inset). This is confirmed by the appearance of magnetic Bragg peaks below  $T_N$  in neutron diffraction data (Fig. 2 upper inset). The magnetization exhibits a small anisotropy, being slightly

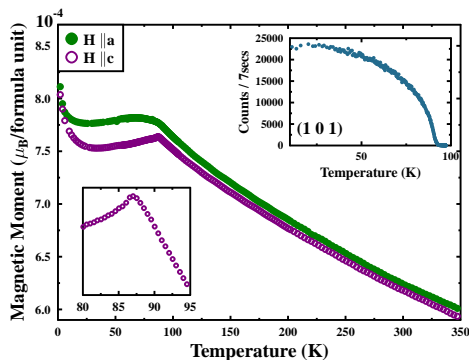


FIG. 2: (Color online) Zero-field-cooled magnetization measurements performed in a magnetic field of strength  $H = 1000$  Oe applied along the  $c$ -axis and  $a$ -axis. The lower inset shows an expanded temperature range about the ordering temperature  $T_N = 87.5 \pm 0.5$  K. The upper inset displays the temperature dependence of the (101) magnetic Bragg peak amplitude.

larger when the field is applied parallel to the  $ab$  plane ( $\chi_{ab}$ ) than along the  $c$ -axis. This easy-plane anisotropy is consistent with the observation that the moments lie in the plane in the ordered phase. The data follows a Curie–Weiss law at high temperatures (not shown) with a negative Weiss temperature,  $\Theta$ . From fits of  $1/\chi$  vs  $T$  we obtain  $\Theta = -819 \pm 2$  K from  $\chi_{ab}$ , and  $-837 \pm 1$  K from  $\chi_c$ . These values are close to those reported previously from single crystals<sup>13</sup>, but somewhat larger in magnitude than obtained from powder samples<sup>35</sup>. A clear cusp is seen at  $T_N$  in  $\chi_c$  whereas a broader peak is seen in  $\chi_{ab}$ . It has been suggested that the cusp in  $\chi_c$  is caused by coupling between adjacent Mn layers, and the more rounded peak in  $\chi_{ab}$  is due to frustration<sup>13</sup>.

Examples of neutron scattering spectra from both instruments are presented in Fig. 3. Figure 3(a) shows energy scans recorded on TASP at the scattering vectors  $\mathbf{Q} = (1, 0, 0)$  and  $(1, 0, 1.5)$ , both of which contain two asymmetric peaks. Figure 3(b) shows data at  $\mathbf{Q} = (1.33, 0.33, 0.5)$  and  $(1.44, 0.11, 0.5)$  measured on 2T1. Since the ordered moment on the Mn sites is relatively large ( $\sim 3 \mu_B$ ) the scattering from magnons is expected to be much stronger than phonon scattering at these relative small scattering vectors. This, together with the resemblance of the spectra to previous measurements on  $\text{YMnO}_3$ , gives us confidence that the main features in the spectra correspond to magnon excitations.

To determine the magnon dispersion we fitted the peaks with Gaussian or Lorentzian functions (depending on the peak shape) on a linear background. The fitted peak positions have been collected together into a dispersion curve which is plotted in Fig. 4, including data from both TASP and 2T1. Measurements on TASP extended

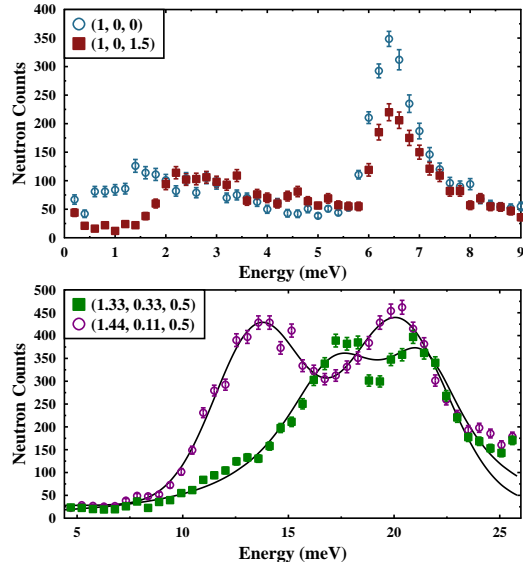


FIG. 3: (Color online) Neutron inelastic scattering from  $\text{LuMnO}_3$  measured on (a) TASP at  $T = 5$  K and (b) 2T1 at  $T = 13.5$  K. The data are from constant-wavevector scans at the indicated positions in reciprocal space. The lines in (b) are fits to a lineshape comprising two gaussian functions.

from below 1 meV up to about 13 meV, while measurements at 2T1 covered the range from about 5 meV up to the energy of the highest modes. Measurements were performed in several different zones to find the maximum intensity and to check that the peaks were periodic in reciprocal space.

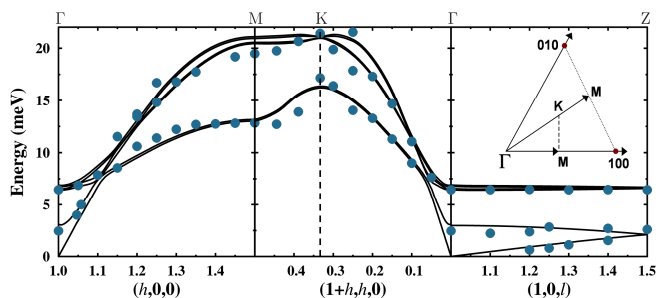


FIG. 4: (Color online) Spin-wave dispersion of  $\text{LuMnO}_3$ . Solid circles are the peak centers obtained from fits to scans such as those shown in Fig. 3. Solid lines are calculated from the model described in the text with parameters  $J_1 = -4.09(2)$  meV,  $J_2 = -1.54(5)$  meV,  $J'_2 = +0.019(2)$  meV,  $J'_1 = 0$ , and  $D = -0.48$  meV. The inset is a sketch of the  $(h, k, 0)$  plane in reciprocal space showing the path  $\Gamma\text{MK}\Gamma$ .

Figure 5 shows diffuse scattering measurements in the vicinity of the point  $(1, 0, 0)$  in reciprocal space at tem-

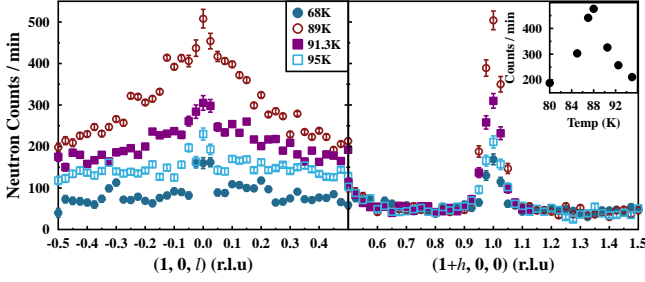


FIG. 5: (Color online) Diffuse neutron scattering around the forbidden nuclear reflection (100). The inset shows the temperature variation in the diffuse scattering intensity at (1, 0, 0).

peratures close to  $T_N$ . The (100) reflection has zero nuclear structure factor, and we observed zero magnetic intensity here at low temperatures. The scans in Fig. 5 reveal strong diffuse scattering at temperatures close to  $T_N = 87.5 \pm 0.5$  with maximum intensity at  $T_N$  itself, as shown in the inset. The diffuse scattering is highly anisotropic, being very broad in the  $(0, 0, l)$  direction but much sharper in the  $(h, 0, 0)$  direction.

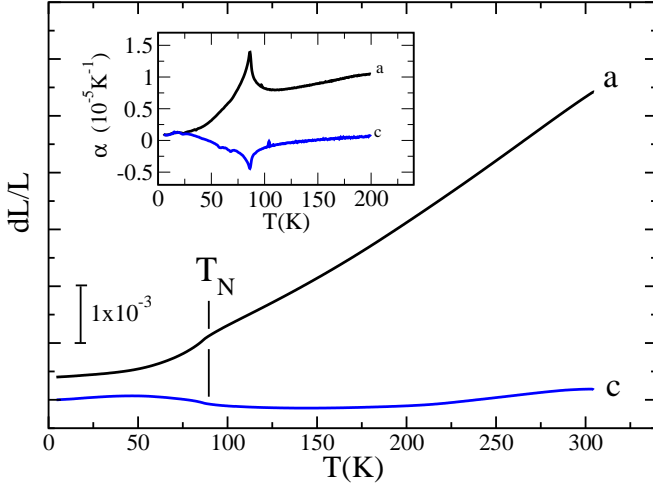


FIG. 6: (Color online) Thermal Expansion of LuMnO<sub>3</sub> measured along the hexagonal  $a$ - and  $c$  directions. The inset shows the thermal expansion coefficient  $\alpha$  as determined from the temperature derivative of the strain  $dL/L$ .

Figure 6 shows measurements of the thermal expansion of LuMnO<sub>3</sub> parallel to the  $a$  and  $c$  axes. A magnetoelectric anomaly is clearly visible at the Néel temperature, both in the strain  $dL/L$  and in its temperature derivative  $\alpha = L^{-1}dL/dT$ . On cooling through  $T_N$  the magnetoelectric strain expands the  $c$  axis and shrinks the hexagonal plane. As a check, we also measured the thermal expan-

sion in the hexagonal plane in the direction normal to  $a$ . The data resemble the behaviour of  $da/a$  to within the experimental error. Above  $T_N$  the thermal expansion is highly anisotropic. The  $c$ -axis strain is almost temperature independent.

#### IV. ANALYSIS AND DISCUSSION

We first review the magnetic structure of the  $RMnO_3$  compounds<sup>14–18</sup>, with particular reference to LuMnO<sub>3</sub>. The six Mn sites in the unit cell (Fig. 1) form two near-equilateral triangles, one in the  $z = 0$  layer and the other in the  $z = 1/2$  layer. The spins on these triangles lie in the basal plane and order in  $120^\circ$  structures. Symmetry constrains the relation between the  $z = 0$  and  $z = 1/2$  layers to two possibilities, conventionally labeled  $\alpha$  and  $\beta$ . In the  $\alpha$  structure the spin on the Mn at  $(x, 0, 0)$  ( $x \approx 1/3$ ) is parallel to that at  $(1-x, 0, 1/2)$ , whereas in the  $\beta$  structure the spins on these two sites point in opposite directions. Each spin makes an angle  $\psi$  to the unit cell axis on which it lies, and the magnetic structure factors depend on  $\psi$  and on the stacking relation ( $\alpha$  or  $\beta$ ). For  $x = 1/3$ , the magnetic structures occur in homometric pairs, such that the magnetic diffraction intensities for the configuration  $(\alpha, \psi)$  are identical with those from  $(\beta, \psi \pm 90^\circ)$ .

In the case of LuMnO<sub>3</sub>, Katsufuji *et al.* concluded from neutron powder diffraction measurements<sup>10</sup> that the low temperature structure is one of two possibilities, either  $(\alpha, \psi = \pm 90^\circ)$  or  $(\beta, \psi = 0^\circ \text{ or } 180^\circ)$ . These two structures transform respectively like the  $\Gamma_4$  and  $\Gamma_2$  irreducible representations of the space group  $P6_3cm$  (Ref. 15). Only this particular homometric pair have a completely absent (100) magnetic reflection. In our single crystal measurements we also found very little intensity at the (100) reflection (but relatively strong intensity for the (101) reflection — see the inset in Fig. 2) at the lowest temperature ( $T = 2$  K), in agreement with Katsufuji *et al.* The homometric pairs can in principle be distinguished by optical second harmonic generation (SHG). Using this method, Fiebig *et al.* found that their sample of LuMnO<sub>3</sub> was a two-phase mixture of  $\alpha$  structures with  $\psi = 0^\circ$  and an unspecified other  $\psi$  value<sup>17</sup>. Since our low-temperature data, as well as that of Ref. 15, conclusively rule out any  $\alpha$  structure which does not have  $\psi \simeq \pm 90^\circ$  it is difficult to see how to reconcile the diffraction and SHG results. For the purpose of modeling the spin wave spectrum we will assume the  $(\alpha, \psi = \pm 90^\circ)$  structure, as shown in Fig. 1. The magnetic spectrum of this and its homometric partner are not distinguishable at the level of precision of our data.

We calculated the spin wave spectrum from the spin Hamiltonian

$$\mathcal{H} = - \sum_{\langle ij \rangle} J_{ij} \mathbf{S}_i \cdot \mathbf{S}_j - D \sum_i (S_i^z)^2, \quad (1)$$

with two in-plane near-neighbor interactions ( $J_1$  and  $J_2$ )

and two inter-plane interactions ( $J'_1$  and  $J'_2$ ) defined as shown in Fig. 1. The first summation in (1) is over pairs of spins with each pair counted once so that the  $J$  constants are per spin pair. The second term models the out-of-plane anisotropy with a single-ion anisotropy parameter  $D$ . We neglect the small in-plane anisotropy since the in-plane magnon gap was too small to measure in our experiment.

Analytic expressions have been given previously for the spin-wave energies derived from spin Hamiltonians similar to (1), Refs. 36–39. These expressions have been obtained via the usual transformation of the Hamiltonian into a quadratic form of boson normal-mode operators in the linear approximation. Here we use an alternative method based on dynamical matrix diagonalisation (DMD) as outlined in previous work<sup>40</sup>, which is implemented in the McPhase software package<sup>41</sup>. This formulation employs the random phase approximation to calculate the magnon cross sections in addition to the dispersion relations.

There are six Mn spins per unit cell, which gives rise to a total of six spin-wave modes for each wavevector. As the interlayer coupling is small, the in-plane dispersion relations appear as three branches each containing two nearly-degenerate modes. The degeneracy of the lowest two modes is lifted close to the  $\Gamma$  point and along  $\Gamma Z$  by the effect of the  $J'_1$  and  $J'_2$  interactions, while the upper four modes are almost degenerate along  $\Gamma Z$ . This degeneracy precludes the possibility to fit accurate values for  $J'_1$  and  $J'_2$  independently, and so we chose to fix  $J'_1 = 0$  and to vary  $J'_2$  under the constraint that  $J'_2 > 0$  to maintain the stability of the  $\alpha$  structure.

A least-squares fitting procedure returned the following values for the model parameters:  $J_1 = -4.09(2)$  meV,  $J_2 = -1.54(5)$  meV,  $J'_2 = +0.019(2)$  meV ( $J'_1 = 0$ ), and  $D = -0.48$  meV. The calculated dispersion relations from the model with these parameters are shown in Fig. 4. The agreement is seen to be very good, and the parameters are well constrained by the data. For example, the 6.5 meV gap to the upper mode at  $\Gamma$  is sensitive to the single-ion anisotropy, and  $J'_2$  controls the dispersion in the out-of-plane direction. The splitting of the magnon peaks in the vicinity of the  $K$  point, seen in Fig. 3, is sensitive to the difference between  $J_1$  and  $J_2$ . Qualitative agreement between the measured and calculated magnon cross sections gave us further support for the obtained parameters.

As a check, we calculated the bulk magnetization using the best-fit exchange and anisotropy parameters. The  $T_N$  predicted by the mean-field model is about 2.5 times larger than the observed  $T_N$ , presumably as a consequence of frustration. The calculated susceptibility has a small easy-plane anisotropy consistent with the measured susceptibility, Fig. 2. The magnetization of the sample as a function of applied field (not shown) is linear and almost identical in the  $a$  and  $c$  directions. Increasing the single-ion anisotropy in the model creates a step in the  $a$ -axis magnetization which is not observed. This adds to the evidence that the single-ion anisotropy is very small

compared to the exchange interactions.

The exchange parameters obtained here show that the dominant magnetic interaction is the in-plane antiferromagnetic superexchange via the  $\sim 120^\circ$  Mn-O-Mn path. The inter-layer superexchange is two orders of magnitude weaker, confirming that the magnetism in LuMnO<sub>3</sub> is highly two-dimensional. It is interesting to compare the magnetic spectrum of LuMnO<sub>3</sub> investigated here with those obtained from similar measurements on YMnO<sub>3</sub> (Refs. 22,31,36,39) and HoMnO<sub>3</sub> (Ref. 38). Qualitatively, the spectra of the three compounds look very similar, but the overall band width of the LuMnO<sub>3</sub> spectrum is about 30% larger than that of YMnO<sub>3</sub> and HoMnO<sub>3</sub> (21 meV compared with 16 meV). Consistent with this, the fitted exchange parameters for LuMnO<sub>3</sub> are found to be systematically larger than those of YMnO<sub>3</sub> and HoMnO<sub>3</sub>. This accounts for the difference in the antiferromagnetic ordering temperatures of these compounds:  $T_N \approx 88$  K (LuMnO<sub>3</sub>) compared with  $T_N \approx 72$  K (YMnO<sub>3</sub>) and  $T_N \approx 75$  K (HoMnO<sub>3</sub>) and the larger Weiss temperature of LuMnO<sub>3</sub> ( $\Theta \approx -850$  K) compared with YMnO<sub>3</sub> ( $\Theta \approx -700$  K)<sup>13</sup>.

The stronger magnetic interactions in LuMnO<sub>3</sub> fits with the systematic trend in the ionic radii and the lattice parameters<sup>10</sup>, i.e. the smaller the ionic radius the smaller the unit cell and the stronger the exchange interactions. The single-ion anisotropy parameter  $D$  is also found to be larger for LuMnO<sub>3</sub> ( $D = -0.48$  meV) than for YMnO<sub>3</sub> ( $D = -0.28$  to  $-0.33$  meV) and HoMnO<sub>3</sub> ( $D = -0.38$  meV). This could be another consequence of the small differences in the structural parameters of these compounds.

The character of the diffuse scattering from LuMnO<sub>3</sub> close to  $T_N$  (Fig. 5) strongly resembles that observed from YMnO<sub>3</sub>.<sup>42</sup> The appearance of scattering which is very broad along  $c$  but relatively sharp in the plane indicates that the inter-layer correlations are very weak, consistent with the small  $J'_1$  and  $J'_2$  and two-dimensional nature of the magnetic system. The strong enhancement in the diffuse scattering intensity around  $(1, 0, 0)$  was also observed in powder diffraction measurements on LuMnO<sub>3</sub>.<sup>10</sup> These showed that the diffuse peak persists up to at least  $\sim 3T_N$ ,<sup>10</sup> which was interpreted as evidence for strong geometric frustration.

Careful powder diffraction measurements<sup>26</sup> have shown that the magnetically-induced ferroelectricity in RMnO<sub>3</sub> is associated with an isostructural transition involving an additional rotation of the MnO<sub>5</sub> bipyramids, and that the increase in ferroelectric polarization below  $T_N$  scales with the square of the ordered moment. The thermal expansion of LuMnO<sub>3</sub> reported here (Fig. 6) reveals a striking magnetoelastic anomaly at  $T_N$ , consistent with the diffraction data of Lee *et al.* (Ref. 26) who argued that magnetoelastic coupling (exchange striction) is the primary source of the magnetoelectric coupling<sup>26</sup>. One might expect, therefore, that the magnetoelectric effect would scale with the strength of the exchange interactions and hence be greater in



LuMnO<sub>3</sub> than in YMnO<sub>3</sub>. Support for this idea is provided by the magnetically-induced polarization calculated from the measured atomic displacements below  $T_N$ , which indeed appears to be systematically larger for LuMnO<sub>3</sub> than for YMnO<sub>3</sub> (Ref. 26). However, given the large experimental uncertainties in the values of the small atomic displacements this evidence should be considered tentative.

Another notable feature of the thermal expansion is how small the  $c$ -axis thermal expansion is relative to the  $ab$  plane expansion above  $T_N$  (see Fig. 6). This effect, which is observed both for LuMnO<sub>3</sub> and YMnO<sub>3</sub>, does not correlate with the compressibility of these materials, which is similar along the  $c$  direction and in the  $ab$  plane<sup>43</sup>. The relatively isotropic compressibility suggests that the anomalous  $c$ -axis thermal expansion is not due to a straightforward anharmonicity in the interatomic potentials along the  $c$  axis, and it would be interesting to find out what is responsible for it.

Before concluding, we investigate the origin of the small magnetic anisotropy of LuMnO<sub>3</sub>, which is represented in the Hamiltonian (1) by the phenomenological  $D(S^z)^2$  term. For reference, we performed a point-charge calculation of the crystal field at the Mn sites assuming Mn to be in the Mn<sup>3+</sup> state with  $d^4$  configuration and using the structural parameters reported by Katsufuji *et al.* in Ref. 10. We included only the five nearest oxygen neighbors of Mn in the MnO<sub>5</sub> bipyramid, as shown in Fig. 7. The ground-state  $S = 2$  manifold is split by the crystal field via the spin-orbit interaction. The calculated splitting, due to the crystal field alone, is also shown in Fig. 7. This model of the crystal field predicts that the ordered magnetic moment points along the normal to the local mirror plane, as shown in Fig. 1, and with the inclusion of the exchange field from the neighboring Mn ions predicts an anisotropy gap in the magnon spectrum of  $\sim 10$  meV. This size of gap is in clear disagreement with the observed spin-wave modes, which have a gap of less than 1 meV at the zone centre, Fig. 4. The anisotropy gap may be reduced in the model if the local symmetry is increased to  $C_{3v}$ , i.e. by lessening the degree of Mn trimerization and tilting of the MnO<sub>5</sub> bipyramid. We conclude, therefore, that the single-ion anisotropy is controlled by a tiny distortion of the ideal MnO<sub>5</sub> bipyramid and that the anisotropy is much smaller than that predicted by a simple point-charge model.

## V. CONCLUSIONS

We have measured the magnon dispersion in LuMnO<sub>3</sub> and achieved a very good description of the spectrum using the Heisenberg Hamiltonian, Eq. (1). We also observed a striking magnetoelastic coupling at  $T_N$  in the thermal expansion. The results are qualitatively simi-

lar to those previously obtained on the sister compound YMnO<sub>3</sub>. The bandwidth of the one-magnon spectrum of LuMnO<sub>3</sub> is about 30% larger than that of YMnO<sub>3</sub>,

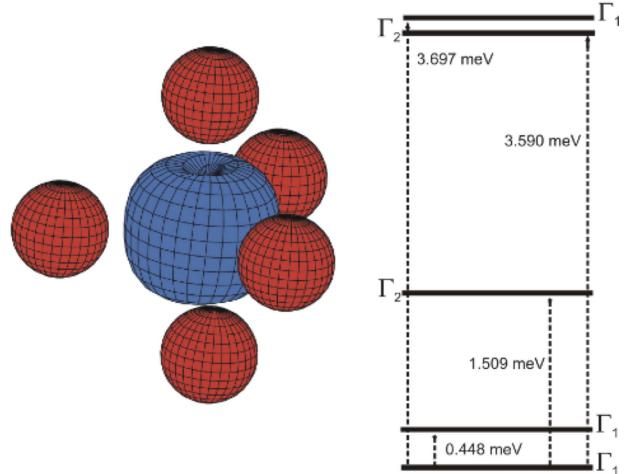


FIG. 7: Left: Calculation of the thermally-averaged charge density in the MnO<sub>5</sub> bipyramid of LuMnO<sub>3</sub> at  $T = 4$  K. The  $3d$  charge is represented (in blue) by a surface of constant charge density obtained from a calculation of the crystal field acting on Mn<sup>3+</sup> assuming point charges of  $-2|e|$  on each of the five nearest oxygen neighbors (shown in red). Right: Low-lying energy levels of Mn<sup>3+</sup> split by the point-charge crystal field via spin-orbit coupling. The symmetry of each level is labeled according to the irreducible representation of the point group  $C_s$ , which describes the local symmetry around the Mn site.

and the difference between the two nearest-neighbour in-plane exchange constants  $J_1$  and  $J_2$  is greater for LuMnO<sub>3</sub> than for YMnO<sub>3</sub>. As the magnetic interactions are stronger in LuMnO<sub>3</sub> than in YMnO<sub>3</sub> we expect the magnetically-induced ferroelectric polarization to be greater in LuMnO<sub>3</sub>. The available diffraction data provides tentative support for this.

## VI. ACKNOWLEDGMENTS

This work was performed partly at the Swiss spallation neutron source SINQ, Paul Scherrer Institut, Switzerland, and partly at the Laboratoire Léon Brillouin, Saclay, France. We are grateful for support from by the Engineering and Physical Sciences Research Council of Great Britain and from the European Commission under the 7th Framework Programme through the ‘Research Infrastructures’ action of the ‘Capacities’ Programme, Contract No: CP-CSA INFRA-2008-1.1.1 Number 226507-NMI3.

- 
- \* Electronic address: a.boothroyd@physics.ox.ac.uk
- <sup>1</sup> T. Kimura, T. Goto, H. Shintani, K. Ishizaka, T. Arima, and Y. Tokura, *Nature (London)* **426**, 55 (2003).
  - <sup>2</sup> N. Hur, S. Park, P. A. Sharma, J. S. Ahn, S. Guha, and S.-W. Cheong, *Nature* **429**, 392 (2004).
  - <sup>3</sup> T. Lottermoser, T. Lonkai, U. Amann, D. Hohlwein, J. Ihlinger, and M. Fiebig, *Nature* **430**, 541 (2004).
  - <sup>4</sup> M. Mostovoy, *Phys. Rev. Lett.* **96**, 067601 (2006).
  - <sup>5</sup> J. J. Betouras, G. Giovannetti, and J. van den Brink, *Phys. Rev. Lett.* **98**, 257602 (2007).
  - <sup>6</sup> S.-W. Cheong and M. Mostovoy, *Nature Mat.* **6**, 13 (2007).
  - <sup>7</sup> M. Fiebig, *J. Phys. D: Appl. Phys.* **38**, R123 (2005).
  - <sup>8</sup> Y. Tokura, *Science* **312**, 1481 (2006).
  - <sup>9</sup> W. Eerenstein, N. D. Mathur and J. F. Scott, *Nature* **442**, 759 (2006).
  - <sup>10</sup> T. Katsufuji, M. Masaki, A. Machida, M. Moritomo, K. Kato, E. Nishibori, M. Takata, M. Sakata, K. Ohoyama, K. Kitazawa, and H. Takagi, *Phys. Rev. B* **66**, 134434 (2002).
  - <sup>11</sup> B. B. Van Aken, T. T. M. Palastra, A. Filippetti and N. A. Spaldin, *Nature Materials* **3**, 164 (2004).
  - <sup>12</sup> Note that there is a discrepancy between different structural studies about whether the Mn shifts to a position with  $x > 1/3$  or  $x < 1/3$ . For  $\text{LuMnO}_3$ , Van Aken *et al.* (Ref. 27) and Lee *et al.* (Ref. 26) report  $x < 1/3$ , whereas Katsufuji *et al.* (Ref. 10) report  $x > 1/3$ .
  - <sup>13</sup> T. Katsufuji, S. Mori, M. Masaki, Y. Moritomo, N. Yamamoto, and H. Takagi, *Phys. Rev. B* **64**, 104419 (2001).
  - <sup>14</sup> E. F. Bertaut and M. Mercier, *Phys. Lett.* **5** 27 (1963).
  - <sup>15</sup> A. Muñoz, J. A. Alonso, M. J. Martínez-Lope, M. T. Casáis, J. L. Martínez, and M. T. Fernández-Díaz, *Phys. Rev. B* **62**, 9498 (2000).
  - <sup>16</sup> W. C. Koehler, H. L. Yakel, E. O. Wollan, and J. W. Cable, *Phys. Lett.* **9**, 93 (1964).
  - <sup>17</sup> M. Fiebig, D. Fröhlich, K. Kohn, S. Leute, Th. Lottermoser, V. V. Pavlov and R. V. Pisarev, *Phys. Rev. Lett.* **84**, 5620 (2000).
  - <sup>18</sup> P. J. Brown and T. Chatterji, *J. Phys.: Condens. Matter* **18**, 10085 (2006).
  - <sup>19</sup> Z. J. Huang, Y. Cao, Y. Y. Sun, Y. Y. Xue, and C. W. Chu, *Phys. Rev. B* **56**, 2623 (1997).
  - <sup>20</sup> A. B. Souchkov, J. R. Simpson, M. Quijada, H. Ishibashi, N. Hur, J. S. Ahn, S.W. Cheong, A. J. Millis, and H. D. Drew, *Phys. Rev. Lett.* **91**, 027203 (2003).
  - <sup>21</sup> K.-J. Jang, J. Lim, J. Ahn, J.-H. Kim, K.-J. Yee, J. S. Ahn, and S.-W. Cheong, *New Journal of Physics* **12**, 023017 (2010).
  - <sup>22</sup> S. Petit, F. Moussa, M. Hennion, S. Pailhès, L. Pinsard-Gaudart and A. Ivanov, *Phys. Rev. Lett.* **99**, 266604 (2007).
  - <sup>23</sup> M. Poirier, F. Laliberté, L. Pinsard-Gaudart, and A. Revcolevschi, *Phys. Rev. B* **76**, 174426 (2007).
  - <sup>24</sup> P. A. Sharma, J. S. Ahn, N. Hur, S. Park, S. B. Kim, S. Lee, J.-G. Park, S. Guha, and S.-W. Cheong, *Phys. Rev. Lett.* **93**, 177202 (2004).
  - <sup>25</sup> S. Lee, A. Pirogov, J. H. Han, J.-G. Park, A. Hoshikawa, and T. Kamiyama, *Phys. Rev. B* **71**, 180413(R) (2005).
  - <sup>26</sup> S. Lee, A. Pirogov, M. Kang, K.-H. Jang, M. Yonemura, T. Kamiyama, S.-W. Cheong, F. Gozzo, N. Shin, H. Kimura, Y. Noda, and J.-G. Park, *Nature (London)* **451**, 805 (2008).
  - <sup>27</sup> B. B. Van Aken and T. T. M. Palstra, *Phys. Rev. B* **69**, 134113 (2004).
  - <sup>28</sup> M. Fiebig, Th. Lottermoser, D. Fröhlich, A. V. Goltsev, and R. V. Pisarev, *Nature (London)* **419**, 818 (2002).
  - <sup>29</sup> A. V. Goltsev, R. V. Pisarev, Th. Lottermoser and M. Fiebig, *Phys. Rev. Lett* **90**, 177204 (2003).
  - <sup>30</sup> E. Hanamura, K. Hagita, and Y. Tanabe, *J. Phys.: Condens. Matter* **15**, L103 (2003).
  - <sup>31</sup> X. Fabréges, S. Petit, I. Mirebeau, S. Pailhès, L. Pinsard, A. Forget, M. T. Fernandez-Diaz, and F. Porcher, *Phys. Rev. Lett.* **103**, 067204 (2009).
  - <sup>32</sup> S. Pailhès, X. Fabréges, L. P. Régnault, L. Pinsard-Godart, I. Mirebeau, F. Moussa, M. Hennion, and S. Petit, *Phys. Rev. B* **79**, 134409 (2009).
  - <sup>33</sup> M. Rotter, H. Mueller, E. Gratz, M. Doerr, M. Loewenhaupt, *Rev. Sci. Instr.* **69**, 2742 (1998).
  - <sup>34</sup> M. Rotter, Patent Nr 502515, Austrian Patent Office.
  - <sup>35</sup> D. G. Tomuta, S. Ramakrishnan, G. J. Nieuwenhuys and J. A. Mydosh, *J. Phys.: Condens. Matter* **13**, 4543 (2001).
  - <sup>36</sup> T. J. Sato, S.-H. Lee, T. Katsufuji, M. Masaki, S. Park, J. R. D. Copley and H. Takagi, *Phys. Rev. B* **68**, 014432 (2003).
  - <sup>37</sup> W. Sikora, O. V. Gurin, and V. N. Syromyatnikov, *J. Magn. Magn. Mater.* **71**, 225 (1988).
  - <sup>38</sup> O. P. Vajk, M. Kenzelmann, J. W. Lynn, S. B. Kim, and S.-W. Cheong, *Phys. Rev. Lett.* **94**, 087601 (2005).
  - <sup>39</sup> T. Chatterji, S. Ghosh, A. Singh, L. P. Regnault, and M. Rheinstädter, *Phys. Rev. B* **76**, 144406 (2007).
  - <sup>40</sup> M. Rotter, *J. Comp. Mat. Sci.* **38**, 400 (2006).
  - <sup>41</sup> McPhase: a software package for the calculation of phase diagrams and magnetic properties of magnetic systems, M. Rotter *et al.*, (2002 – 2010), available at <http://www.mcphase.de>.
  - <sup>42</sup> B. Roessli, S. N. Gvasaliya, E. Pomjakushina, and K. Conder, *JETP Lett.* **81**, No. 6, 287, (2005).
  - <sup>43</sup> D. P. Kozlenko, S. E. Kichanov, S. Lee, J.-G. Park, V. P. Glazkov and B. N. Savenko, *JETP Lett.* **82**, 193 (2005).